



UNIVERSITÀ POLITECNICA DELLE MARCHE
Repository ISTITUZIONALE

High-Pressure-Driven Reversible Dissociation of alfa-Synuclein Fibrils Reveals Structural Hierarchy

This is a pre print version of the following article:

Original

High-Pressure-Driven Reversible Dissociation of alfa-Synuclein Fibrils Reveals Structural Hierarchy / Piccirilli, Federica; Plotegher, Nicoletta; Ortore, Maria Grazia; Tessari, Isabella; Brucale, Marco; Spinozzi, Francesco; Beltramini, Mariano; Mariani, Paolo; Militello, Valeria; Lupi, Stefano; Perucchi, Andrea; Bubacco, Luigi. - In: BIOPHYSICAL JOURNAL. - ISSN 0006-3495. - STAMPA. - 113:8(2017), pp. 1685-1696. [10.1016/j.bpj.2017.08.042]

Availability:

This version is available at: 11566/251853 since: 2022-06-01T12:17:37Z

Publisher:

Published

DOI:10.1016/j.bpj.2017.08.042

Terms of use:

The terms and conditions for the reuse of this version of the manuscript are specified in the publishing policy. The use of copyrighted works requires the consent of the rights' holder (author or publisher). Works made available under a Creative Commons license or a Publisher's custom-made license can be used according to the terms and conditions contained therein. See editor's website for further information and terms and conditions.

This item was downloaded from IRIS Università Politecnica delle Marche (<https://iris.univpm.it>). When citing, please refer to the published version.

(Article begins on next page)

High Pressure driven reversible unfolding of alpha-synuclein fibrils reveals structural hierarchy in their formation

F. Piccirilli[§], N. Plotegher[§], M. G. Ortore, I. Tessari, F. Spinozzi, M. Beltramini, P. Mariani, V. Militello, S. Lupi,
A. Perucchi, L. Bubacco*

§ These two authors equally contributed to this work.

KEYWORDS: amyloid fibrils, high pressure, FTIR, Raman, dissociation, Parkinson's disease

Running title: Unfolding of alpha-synuclein fibrils

* To whom correspondence should be addressed: luigi.bubacco@unipd.it

ABSTRACT

The analysis of the alpha-synuclein (aS) aggregation process, which is involved in Parkinson's disease etiopathogenesis, and of the structural feature of the resulting amyloid fibrils may shed light on the relationship between aS aggregates structure and their toxicity. This may be considered a paradigm of the ground work needed to tackle the molecular basis of all the protein aggregation-related diseases.

With this aim, we used chemical and physical dissociation methods to explore the structural organization of wild type (wt) aS fibrils. High pressure (in the kbar range) and alkaline pH were used to disassemble fibrils to collect information on the hierarchic pathway by which distinct β -sheets sequentially unfold using the unique possibility offered by high pressure Fourier transform infrared spectroscopy (FTIR).

The results point toward the formation of kinetic traps in the energy landscape of aS fibrils disassembly and the presence of transient partially folded species during the process. Since we found that the dissociation of wt aS fibrils by high pressure is reversible upon pressure release, the disassembled molecules likely retain structural information that favours fibrils reformation. To deconstruct the role of the different regions of aS sequence in this process, we measured the high pressure dissociation of amyloids formed by covalent chimeric dimers of aS (syn-syn) and by the aS deletion mutant lacking the C-terminal, i.e. aS(1-99). The results allowed to single out the role of dimerization and of the C-terminal in the complete maturation of fibrillar aS.

Introduction

α -synuclein (aS) is a 140 aminoacids (aa) protein mainly expressed at pre-synaptic terminals in the mammalian central nervous system. It can be divided in three domains: the amphipathic N-terminal region (1-60 aa), which acquires an α -helical structure when bound to lipid membranes(1); the non β -amyloid component (NAC) (61-95 aa), which is highly hydrophobic and involved in aS aggregation(2); the C-terminal (96-140 aa), which is highly acidic and has no distinct structural features. aS monomers has been first described as natively unfolded protein in solution, even if tetrameric α -helical forms were observed(3). It has been also shown that the structure of monomeric aS in solution is more compact than expected for a completely unfolded polypeptide. In fact, long range interactions between the C-terminal region and the hydrophobic NAC domain have been proposed to stabilize aS in the monomeric state *in vitro*(4) and in mammalian cells(5).

The physiological functions of aS are not fully understood, but several studies suggest a role in synaptic vesicles recycling(6, 7), SNARE complex assembly(8) and neuronal plasticity(9). Great efforts have been made to characterize structural and functional properties of aS after the discovery of the link between aS aggregation and Parkinson's disease (PD)(10). A β -sheet rich fibrillar form of aS is the major component of Lewy bodies (LBs)(11), which are intracellular deposits of proteins and lipids found within surviving neurons in brains of patients affected by PD or by other synucleinopathies(12). The structure of aS amyloid fibrils was studied by X-ray diffraction, solid state NMR and cryo-electron microscopy(13)(13–15), , and by micro-electron diffraction(16) down to atomic resolution. The results suggested a cross- β structure, similar to other amyloid fibrils, in which the β -sheets motives are oriented perpendicularly to the fibril axis. However, the structural details of fibrillar aS represent the ground on which to construct a classification of the divers strains reported in the recent literature(17) and associated to different phenotypes traits.

The early stage of aS aggregation is an oligomerization process, where few monomers assemble to form transient and heterogeneous oligomeric species. Fibrillar structures are then formed through successive additions of monomers or other oligomeric species to the growing aggregates. During the process several distinct transient oligomeric and protofibrillar species seem to populate the system (for a review of aS aggregation process see Plotegher et al. 2014)(18). The aS oligomers can be conceived either as on- or off-

pathway intermediates in fibril formation. In the attempt to define the toxic forms of aS, oligomers were shown to be responsible for neurons death(19). However, neuronal death was also associated to the presence of LBs, while neurons with no inclusions seem to be less vulnerable(20). Given the heterogeneity of the different aS aggregates and the proposed toxic effects assigned to both aS oligomers and fibrils, the molecular mechanisms of cytotoxicity of aS aggregates remain elusive as the structural features that govern them.

Therefore, in spite of their relevance in neurodegeneration, the structural information on the several aggregation intermediates of aS is still scanty and difficulties arise when trying to identify those that are relevant for the *in vivo* aggregation process and for the pathology. This can be rationalized considering the several technical limitations due to the heterogeneous and transient nature of oligomeric intermediates, which hinders the isolation of the individual components. However, ensemble measurements, such as Circular dichroism (CD) and infrared (IR) spectroscopy indicated that most of the on-pathway aS oligomeric intermediates contain substantial β -sheet structure(21).

An alternative avenue of investigation starts from the analysis of the end products, i.e. mature aS amyloid fibrils. These structures show a substantial thermodynamic stability and previous studies associated fibrils structural inertia to the involvement of several weak interactions, such as hydrophobic effect, π - π interactions and ion pairing among amino acid side chains. It is now well accepted that amyloids fibrils can be destabilized(22) or even completely dissociated(23) by tuning the net charge of the polypeptide chain. For example, aS fibrils disassemble into monomeric units in a very alkaline environment(24), or when subjected to low temperature which weakens electrostatic interactions and hydrophobic effects(25, 26). An alternative strategy to obtain a controlled reversible dissociation of amyloid fibrils, based on the fine-tuning of weak interactions, is high hydrostatic pressure (HP)(27–30). It was observed that pressures around 2 kbar dissociates aS fibrils(27, 30), by forcing the equilibrium toward dissociation. High pressure shifts the system towards the state that occupies the minimum achievable volume, which is reached by solvent electrostriction around charged groups and is associated to important water density changes. The latter affects the intensity of the hydrophobic effect(31), ion pairs dissociation and exposure of hydrophobic surface to solvent. Therefore, using kbar pressures, it is feasible to finely tune weak interactions, inducing

partial or total disassembling of the tertiary structure and even a cooperative unfolding of the H-bond wires of the protein secondary structure.

Here we present a FTIR and Raman characterization of the high pressure (in the kbar range) and pH driven dissociation of wild type (*wt*) aS fibrils with the goal of providing a structural characterization of aggregation intermediates and the processes which may be relevant in defining new methods to interfere with the aggregation and its associated toxicity. The disassembly seems to follow a hierarchic pathway where distinct β -sheets unfold sequentially. The results point toward the formation of kinetic traps in the energy landscape of aS fibrils disassembly, explored using the unique possibility offered by high pressure FTIR to characterize transient partially folded species. In an attempt to deconstruct the role of the different regions of aS in fibrils stability, we measured the high pressure dissociation of amyloids formed by covalent chimeric dimers of aS (syn-syn)(32) and by the aS deletion mutant lacking the C-terminal, i.e. aS(1-99).

Materials and Methods

Proteins purification

The syn-syn dimer, constituted by the amino acids 1-104 and 29-140 of aS cloned in tandem, *wt* aS and C-terminal depleted aS(1-99) were all expressed and purified as described elsewhere (respectively Pivato *et al.* for the first(32), Plotegher *et al.* for the second(33) and Bortolus *et al.* for the deletion mutant(34)).

Briefly, proteins were expressed into *E. Coli* strain BL21(DE3). For *wt* aS and syn-syn dimer, cells were grown at 37°C in LB medium to an OD₆₀₀=0.03-0.04 and induced with 0.1 mM isopropyl β -thiogalactopyranoside for 5 hours. Cells were then collected and the recombinant proteins were recovered from the periplasm by osmotic shock. The periplasmic homogenate was then boiled for 15 minutes and the soluble aS-containing fraction was subjected to a two-step (35% and 55%) ammonium sulphate precipitation. The pellet was re-suspended, dialyzed against 20 mM Tris-HCl pH 8.0, loaded into a 6 ml Resource Q column (Amersham Biosciences) and eluted with a 0-500 mM gradient of NaCl.

aS(1-99) overexpressing cells were grown at 37°C in LB to an OD₆₀₀=0.08 and induced with 0.3 mM isopropyl β -thiogalactopyranoside. After 4 hours, homogenized cells were boiled for 15 minutes and ammonium sulphate was added to the soluble fraction in two steps (35% and 55%). The resuspended pellet was

dialyzed and loaded into a 6 ml Resource S column (Amersham Biosciences) and eluted with a 0-500 mM NaCl gradient. Finally, all the proteins were dialyzed against water, lyophilized and stored at -20 °C.

Fibrils preparation

Proteins were resuspended into deuterated PBS pH 7.4 and filtered with a 0.22µm filter to eliminate residual aggregates due to lyophilisation. Soluble proteins were quantified using a UV-visible diode-array (Agilent 8453); absorbance was measured at 280 nm and protein concentration calculated using protein molar extinction coefficient corresponding to $\epsilon(\text{aS})=5960 \text{ M}^{-1} \text{ cm}^{-1}$, $\epsilon(\text{syn-syn})=7450 \text{ M}^{-1} \text{ cm}^{-1}$ and $\epsilon(\text{aS}(1-99))=1490 \text{ M}^{-1} \text{ cm}^{-1}$. Fibrils were obtained by aggregating the solubilized proteins at a concentration of 6 mg/ml, to which NaN_3 to a final concentration of 0.05% was added. After 1 week at 37°C under shaking at 1000 rpm, fibrils were collected by pelleting for 2 hours (15000g) and the residual soluble aS in the supernatant was quantified as reported above.

The amount of aS converted to fibrils was calculated as the difference between the initial amounts used in the aggregation assay and the residual protein present in the supernatant. Fibrils were then re-suspended in a proper volume of deuterated PBS, 0.05% NaN_3 to a final equivalent monomeric concentration of 10 mg/ml.

TEM imaging

TEM samples were prepared by adsorbing a 15-20 µl aliquot of aggregated proteins samples (monomeric equivalent concentration about 0.3mg/ml) onto a carbon-coated copper grid. Negative staining was performed with 0.05% uranyl acetate solution. TEM images were acquired on a Tecnai G2 12 Twin instrument (FEI Company, Hillsboro, OR).

FTIR Measurements

High-pressure FTIR measurements were performed with a conventional infrared interferometer (IFS66 - Bruker) coupled to the infrared microscope (Hyperion - Bruker). The samples were loaded into a diamond anvil cell (DAC) equipped with IIa diamonds with a culet of 600 µm. A gasket of stainless steel 40 µm thick has been used.

Ambient pressure measurements were performed using a standard liquid cell equipped with CaF_2 windows (2mm thick) separated by a spacer of mylar 40 µm thick. Data were analyzed by using OPUS Pro 6.5 (Bruker

Optics). 2nd-derivative spectra have been calculated with the *Savitzky-Golay algorithm* and 17-smoothing points. A homemade fluorescence system(28) based on the ruby fluorescence technique was used for pressure calibration. The kinetic evolution of Amide I' band, in high pressure and pH jump experiments, was followed for 40 minutes by starting the measurements cycle immediately after pressure increase and pH change, having each measurement a duration of 2 minutes. FTIR measurements at constant pressure have been acquired at signal equilibration after pressure increase.

Micro-Raman Measurements

Micro-Raman (μ -Raman) measurements were performed with a Bruker SENTERRA microscope equipped with a 532 nm Laser (Nd:YAg) used at a power of 20 mW. Spectra were acquired on lyophilized samples in the spectral range of Amide I and Amide III bands ($1750\text{-}1200\text{ cm}^{-1}$) with a resolution of 3 cm^{-1} .

Circular dichroism (CD) Spectroscopy

CD experiments were performed on a JASCO J-715 spectropolarimeter equipped with HELLMA quartz cells with Suprasil® windows and an optical path length of 0.1 cm. CD spectra were acquired at room temperature and processed using the manufacturer software. All spectra were recorded in the wavelength range of 200-250 nm, using a bandwidth of 2 nm and a time constant of 2 s at a scan speed of 50 nm/min. A single spectrum was acquired every 5 minutes from the addition of 5 μl NaOH 1M to the initial fibrils solution of 150 μl (final pH 11).

Results and Discussion

High pressure versus pH dissociation of aS fibrils.

Aiming to define the structural features that govern the formation of wt aS fibrils we analysed the disassembly process as induced by alkaline pH and HP. Both experiments started from aS fibrils formed at physiological pH. Their fibrillar state was validated by thioflavin assay and TEM. The alkaline dissociation was obtained by re-suspension of the pelleted fibrils in a basic solution (pH 11), while the pressure-controlled dissociation required the use of an optical diamond anvil to reach the reported pressures (up to 2.6 kbar). FTIR spectroscopy was used to describe the secondary structure variations occurring during the dissociation experiments. The structure assignments of IR peaks, performed in accordance with literature

data (28, 35), are reported in Table 1. The amide I band of aS fibrils at atmospheric pressure and neutral pH (Figure S1) shows a prominent narrow peak at about 1617 cm^{-1} , hallmark of intermolecular β -sheet(35) and a broad shoulder covering the spectral region $1630\text{-}1680\text{ cm}^{-1}$, where intramolecular structures absorb. Figure 1 shows the time evolution of the band upon HP- and pH-induced dissociation of fibrils (panel A and B, respectively). The narrow feature of intermolecular β -sheet at 1617 cm^{-1} decreases under both disassembly conditions. Conversely, the signal ascribed to random coil and other intramolecular structures, absorbing in the region $1645\text{-}1660\text{ cm}^{-1}$ increases.

A remarkable property of the HP-induced dissociation is the presence of only two main species, as suggested by the presence of an isosbestic point, reported also by other groups (27, 30), observed at 1630 cm^{-1} . Moreover, we also compared the Amide I' band at pressure release to the one acquired before pressurization to evaluate the reversibility of the dissociation process (see *Figure S1*). Interestingly, while fibrils dissociation is reversible, being that the initial absorption spectrum of fibrillar β -sheet (around 1617 cm^{-1}) is fully restored, small structural changes concerning turns and other non-fibrillar moieties(35) or small lateral chains rearrangements(36) are signalled by the slight absorption decrease in the region around 1685 cm^{-1} . A possible interpretation implies the presence of a small amount of amorphous aggregates in the pressure untreated sample that could be easily dissociated by high pressure. This data interpretation is in accordance to experimental evidences that establish the enhanced sensitivity of amorphous aggregates to high pressure compared to amyloids(37).

While both HP and pH jump experiments lead to the dissociation of β -sheet (β) into random coil and intramolecular structures (r) (Figure 1), only the dissociation induced by alkaline pH causes the appearance of a substantial and novel feature at 1685 cm^{-1} in the spectra, which was previously assigned to β -turn moieties and non-amyloid aggregates(38). The very narrow bandwidth of this feature suggests the formation of highly ordered structures and its spectral position is compatible with an attribution to turns and strands in aggregated structures and/or to COO^- stretching in H-bonded lateral chains(38, 39). The end product of the alkaline disassembly cannot be reverted to fibrils and it is likely an amorphous aggregate, posing a question on the interpretation of dissociation studies on aS fibrils solely based on alkaline pH.

2D-COS analysis of HP- and pH-driven dissociation process

Further information on the two disassembly processes can be acquired using the 2D-COS analysis reported in Figure 1 (panels C-E for HP-dissociation and panels D-F for pH-dissociation) and Table 2. In this type of analysis, the real part of the autocorrelation function, the synchronous spectrum (Φ) provides information on the correlation among changes of measured spectral series. The off diagonal peaks represent the degree of correlation between spectral features changes. Positive peaks are thus generated for spectral features in which the intensity variations occur in the same direction (for example, both increasing), while negative peaks report intensity variations in opposite directions.

The imaginary part of the autocorrelation function, the asynchronous spectrum (Ψ), detects sequential changes of measured spectral series instead. Between the two spectra, the asynchronous spectrum is of particular interest because it allows the distinction of spectral intensity changes, which occur out-of-phase (i.e. delayed or accelerated), as a function of time. In positive synchronous correlation between two spectral features, positive asynchronous cross-peaks indicate that the first feature of the correlation couple $k_1:k_2$ changes earlier or more significantly than the second feature. This trend is reversed for negative synchronous features. Therefore, the asynchronous maps allow the distinction of individual spectral features composing Amide I' band, corresponding to the secondary structure moieties, which are involved in the two dissociation processes. The secondary structures derived from this analysis are reported in Table 1 while correlation peaks frequencies and the respective data interpretation are reported in Table 2. The correlation analysis applied to HP dissociation process (see Figure 1C-1E) shows a complex pathway of structural reorganizations. It confirms the conversion of β -sheet into random coils and suggests the presence of two processes occurring in parallel: 1) fibrillar β -sheet dissociate into shorter intermolecular β -sheet, possibly oligomeric, then into random coil; 2) fibrillar β -sheet dissociation leads to the increase in bends, turns and, eventually, random coils.

The first is a “fragment-mediated dissociation” in which the disassembly of fibrils to shorter β -sheet fragments of few peptides, likely oligomeric species, eventually leads to the complete dissociation into random structures.

The second is a “direct dissociation” of peptides involved in the conversion of fibrillar β -sheet into random coils in which only fractions of the polypeptide chain unfolds at each pressure step. The presence of a broad asynchronous anti-correlation peak centred at about $1685\text{-}1618\text{ cm}^{-1}$, covering also the spectral region around $1685\text{-}1622\text{ cm}^{-1}$, suggests that the coupled peaks change at different times. This piece of evidence allows to rule out the correspondence of the peak at 1685 cm^{-1} to the high frequency component of antiparallel β -sheet, and to assign it to turns, aggregated strands or lateral chains (40,41). However, since the high frequency peak enabling to resolve β -sheet reciprocal arrangements has typically a small intensity, further investigation is required to establish whether aS molecules in the observed aggregates are in a parallel or anti-parallel fashion. For these reasons, we associated the correlation peaks $1685\text{-}1618\text{ cm}^{-1}$, $1685\text{-}1622\text{ cm}^{-1}$ (coupling the component at 1685 cm^{-1} to β -sheets in fibrils and in oligomers, respectively) to small variations in turns, aggregated strands or lateral chains arrangements while fibrils dissociate. All these assignments are compatible with the presence of a small amount of amorphous aggregates in the sample before the pressure treatment. Signals associated to lateral chains, i.e. the asynchronous correlation signals at 1605 and 1612 cm^{-1} , considered typical hallmarks of tyrosine, suggest a reorganization of these chains during the dissociation.

A rationalization of the process of the “direct dissociation” was attempted by considering the structure of aS fibrils predicted by the experiments reported in the literature. As suggested by solid state NMR, EPR and AFM experiments, aS fibrils structure is composed by a cluster of few distinct β -sheets(18). In Figure 1A we showed that the amide I' mode associated to β -sheet was already in an intermediate state at the beginning of the kinetics at 2.6 kbar, with a lower content of β -structures in comparison with fibrils at the ambient pressure. Moreover, the sample shows a detectable content of β -sheet once equilibrium is reached (a shoulder at about 1619 cm^{-1} is still present at the longest time explored, i.e. 2 hours, and up to the maximal reached pressure). This result suggests that only a fraction of β -sheet is susceptible to the applied pressure providing further support to the already established sequential action of higher pressures on proteins structure(28).

In the “fragment-mediated dissociation” scheme, the β -sheets that constitute the fibrils are converted into shorter structures, possibly oligomeric forms, tentatively assigned to the 1622 cm^{-1} feature. It was recently

reported(42) that amyloid fibrils formed from the SH3 domain of the α -subunit of phosphatidyl inositol-3'-kinase are not stable static structures but could rather be considered as reservoirs from which oligomers could attach and detach leading to a turnover of molecules within the fibril population. Therefore, we can suggest that when fibrils are subjected to high-pressure the system shifts towards the state with the smaller volume, favouring the detachment of individual oligomers from the fibrils. An analogous process could be at the basis of the intermediate misfolded aS forms found here at high pressure (short β -sheet signals at 1622 cm^{-1})(35).

The latter observation implies that at high pressure kinetic traps are stabilized in the energy landscape. The presence of intermediate states detected during HP fibrils dissociation is in agreement with the off-lattice minimalist model proposed by Hillson *et al.*(43) and developed for a β -barrel protein, which establishes the enhancement of the overall roughness of the energy landscape at high pressure. The reversibility of the HP dissociation suggests also that the HP intermediate states become energetically unfavourable upon pressure release. The fast kinetic of the reassembly implies that the intermediates retain sufficient structural information to efficiently drive the process. Despite the relevance in the understanding of structural features that may be responsible for aS aggregates toxicity, it remains to be proved that the intermediates observed *in vitro* are of relevance for the *in vivo* process of aggregation.

The correlation features observed for pH dissociation allow us to describe the process as follow: highly ordered structures dissociate into random coils ($\beta_{\text{fibril}}:r$ 1617:1645 cm^{-1}) and turns ($(\beta_{\text{fibril}}:t$ 1617:1658 cm^{-1}) and then re-aggregate ($\beta_{\text{fibril}}:t,b$ 1617:1685 cm^{-1}). The lack of intermediate steps in pH dissociation can be explained by considering that when aS is subjected to an alkaline pH, it acquires a strong global negative charge, shifting from -9 at neutral pH to -27 at pH 11. The additional charge acquired by the protein is likely due to the deprotonation of lysine ($\text{pK}_a = 10.53$) and tyrosine ($\text{pK}_a = 10.07$) residues. Considering that 10 of the 15 lysine residues in the aS sequence are placed in solvent protected regions of the amyloid(15, 44), it is conceivable that, at least within the time scales of FTIR experiments, pH dissociation occurred through the one-step dissociation of the whole β -sheet structure. Moreover, the tertiary reorganization of the protein due to the electrostatic charges stabilization possibly induces the collapse of the unfolded ensemble and leads to an unspecific irreversible aggregation.

aS fibrils pH-induced dissociation studied by Raman spectroscopy

To further investigate the nature of the specie obtained by pH dissociation we performed Raman experiments. Raman spectra in the region of Amide I and Amide III bands are reported in Figure 2A-2B. The dissociation of fibrils already observed in IR experiments is confirmed by the spreading of the main Raman peak at about 1660 cm^{-1} (45). As suggested by the Amide I band, similarities between monomeric aS and pH-dissociated fibrils, no variations in secondary structure occur during the final re-aggregation process. The presence of the peak at 1603 cm^{-1} , associated to tyrosine residues ring modes, in the spectra of alkaline pH-treated samples suggests that fibrils dissociation is linked to a re-organization of tyrosines. Important information can be obtained from the region around Amide III band. The shape of the bands in the region between $1280\text{-}1230\text{ cm}^{-1}$ confirms what inferred by Amide I' observation: fibrillar β -sheet decreases during alkaline pH treatment and secondary structure of monomeric aS and alkaline pH treated fibrils are strictly similar. Furthermore, the intensity increase and the narrowing of the peak at about 1405 cm^{-1} , associated to C_{β} modes and previously assigned to COO^- stretching of acid lateral chains(45), suggests an ordering of carboxylic groups in the structures obtained upon alkalization. The presence of this peak in the pH-dissociated fibrils together with the evidence of an IR feature at about 1685 cm^{-1} suggests that the ordering of acid residues may be involved in the formation of H-bonds of aggregated structures formed upon alkanisation. The decrease in β -sheet content upon alkaline pH treatment was independently assessed by CD (Figure 2C) and confirms the progressive loss of secondary structure. TEM measurements performed on the sample after exposure to pH 11 confirmed the aggregated and amorphous nature of the end products (Figure 2D).

High pressure dissociation of syn-syn and aS(1-99) chimeric mutants

Among the several factors affecting aS aggregation propensity, protein intramolecular diffusion and conformational flexibility govern the early stages of the process, when the early products of aggregation are oligomers(46). For this reason, we also studied the response to high pressure of fibrils formed from a chimeric aS covalent dimer(32)with a double NAC region (syn-syn dimer). Interestingly, aS covalent dimers formation has been reported in the literature as product of redox chemistry(47–49). Furthermore, it has

been observed that in chimeric aS covalent dimers the conformational constraints imposed by dimerization can strongly affect their aggregation propensity(32).

A second important role in the aggregation/stability of aS fibrils is played by the C-terminal region(50). It has been suggested that rearrangements at the C-terminal occur early during the aggregation process(51). Moreover, C-terminal truncated forms of aS aggregate faster than *wt* aS(51) and the resulting fibrils are smaller in diameter compared to the aS mature fibrils. It has been recently reported(25, 26) that amyloid fibrils can be reversibly dissociated or destabilized at low temperature as a result of the weakening of charge intensity on lateral chains. Ikenoue *et al.*,(26) observed remarkable differences in low temperature stability of *wt* and C-truncated aS fibrils, suggesting a possible role of the burial of negative charges in fibril cores as responsible for the cold denaturation of aS fibrils. This may result from the increase in the electrostatic repulsion at low temperature due to the increases in the dielectric constant and in hydrophobic hydration. By comparing the effects of low temperature and high pressure on proteins, it seems clear that there are many similarities in the dissociation process they trigger, since they both act mainly by decreasing weak interactions.

On these bases, we analyzed the high pressure behaviour of fibrils formed by the syn-syn dimer and the C-terminal depleted mutant aS(1-99).

Figure 3A-3B reports the equilibrium Amide I' band of these two chimeric mutants upon compression. The dissociation of β -sheet structures is shown by the decrease of the absorption around 1620 cm^{-1} , coupled with the increase of random coil and intramolecular structures moieties absorbing around 1645 cm^{-1} .

Interestingly, several steps toward high-pressure are required to completely dissociate amyloid fibrils (up to 5.2 kbar for aS(1-99) and to 3.3 kbar for syn-syn). Moreover, one isosbestic point drawn by Amide I' high pressure bands appears around 1634 cm^{-1} in aS(1-99) compression experiment and around 1631 cm^{-1} for syn-syn dimer.

The 2D-Correlation analysis performed on the high pressure dissociation kinetics of the two species (Figure S2) shows two parallel pathways of dissociation, a “direct dissociation” and a “fragment mediated dissociation”, confirming the description of the overall process presented above for *wt*aS fibrils (Figure 1). Interestingly, the presence of the two β -sheet species, building up fibrils (1618 cm^{-1}) and oligomers (1621

cm⁻¹), is clearly resolved also in the synchronous spectrum of the chimeric dimer fibrils (Figure S2). This effect can be ascribed to the enhanced structural order in dimers likely due to covalent constraints. In order to get a more quantitative description of this dissociation process for syn-syn and aS(1-99) fibrils, we considered the decrease of the signal associated to β -sheet moieties as a function of pressure (Figure 3C), which can be associated with the percentage of fibrillar proteins in the sample. To get indicative values for the pressure at which amyloids are dissociated, we model the data with sigmoid profiles (Figure S3), introducing the dissociation pressure P_d as the value at which β -sheet signal is reduced of 50%. It is worth noting that the Amide I' of syn-syn fibrils and the C-depleted mutant aS(1-99) fibrils at atmospheric pressure are different (Figure S4), reflecting substantial differences in secondary structure.

Interestingly, syn-syn dimers fibrils show a P_d value close to the one experimentally obtained by Foguel *et al.* (27) for wt aS, around 2 kbar. This suggests that structural and volumetric properties of fibrils are not affected by the covalent constraints imposed by dimerization. Moreover, as suggested by the shape of the dissociation curve in Figure 3C, syn-syn β -sheets dissociation occurs in one main step, similarly to what found for wt aS. Conversely, by observing the atmospheric pressure Amide I' band measured for aS(1-99) amyloid (Figure S4), we can speculate on the occurrence of at least two steps of dissociation taking place during aS(1-99) fibrils compression, in which β -sheets result less susceptible to high pressure, showing a P_d around 3.3 kbar.

The different behaviours observed between syn-syn dimer and the C-depleted mutant aS(1-99) can be explained by considering the morphology of the two types of fibrils that they generate. While aS(1-99) does not show the tendency to form mature fibrils(51) and mainly forms protofibrils, covalent syn-syn dimers can aggregate up to mature fibrils(32). As reported in the literature(15, 51, 52), aS protofibrils are formed by two protofilaments and the side interactions between protofibrils have a fundamental role in the formation of mature fibrils. In the syn-syn dimers, this interaction between protofibrils is preserved, although the resulting mature fibrils exhibit a non-homogenous distribution of heights and a reduced average length compared to wt aS(32). Thus, the similarities observed in response for wt aS and syn-syn aggregates to high pressure reflect the fact that both proteins can form mature fibrils upon aggregation. Conversely, C-terminal

depletion hinders the formation of mature fibrils and this changes the response of aS(1-99) to high pressure.

Moreover, the presence of more than one step of dissociation for aS(1-99) may reflect the presence of different populations of β -sheet in the structure: protofilaments and protofibrils.

Information about the hardness of β -sheet in each sample can be obtained from the observation of absorption frequencies around 1620 cm^{-1} . β -sheet absorption frequencies strongly depend on transition dipole coupling effects and on H-bonds. These frequencies are affected by the deuteration state of the chain and by structural parameters, like the number of residues in the strands and the number of strands per sheet. In particular, the Amide I absorption frequency is inversely proportional to the number of strands per β -sheet(35).

Figure 4 reports the 2nd-derivative spectra of chimeric mutants recorded at atmospheric and high pressure.

As it can be inferred by the position of 2nd-derivative minima, β -sheet in syn-syn dimers fibrils absorbs around 1620 cm^{-1} . Upon compression we did not observe any shift of β -sheet moiety in syn-syn amyloids.

Considering that in the explored range of pressure the occurrence of spectral shifts of vibrational modes upon compression should report mechanical deformation of hydrogen bonds, the absence of shifts in syn-syn fibrils suggests that β -sheet in dimers are disassembled by high pressure without being subjected to structural deformations. The structure of aS(1-99) fibrils appears to be composed of two distinct β -sheet populations, as reported by the minima in 2nd-derivative spectra observed around 1623 and 1614 cm^{-1} . An assignment coherent with the interpretation of the high-pressure dissociation profile reported in Figure 4.

Upon compression of aS(1-99) fibrils, β -sheet high frequency component (1623 cm^{-1}) undergoes blue-shift while the low frequency one (1614 cm^{-1}) red-shifts, up to a pressure of 4.5 kbar at which the two components overlap. A rearrangement of β -sheet, which results in reducing (blue-shift) or increasing (red-shift) H-bond distances, can rationalize these effects and may take place in response to the overall volume reduction induced by high pressure. As it can be observed in 2nd-derivative spectra (Figure 4) of both samples, intra-chain H-bonds and random coiled structures are mainly stabilized at the maximum pressure applied (i.e. 5 kbar), as revealed by minima in the region $1660\text{-}1640\text{ cm}^{-1}$, with a minor contribution of residual β -sheet. Upon pressure release, the initial signal completely restores also for chimeric mutants,

suggesting the reversibility of the process. To verify whether the reversibility of the process restores not only the β -sheet structure of the fibrils, but also higher fibrils morphological features, we recovered the protein from the high pressure cell after a compression-decompression cycle. As shown in figure S5, aS(1-99) fibrils maintain their morphological characteristics after the HP treatment, substantiating the complete reversibility of the process. The overall reversibility of the HP induced unfolding of the divers aS fibrils reported here, does not align with the recent observation by Oliveira *et al.*, (30) that fibrillary aS dissociate to monomer and does not go back for fibrillary form upon pressure release. The longer exposure to high pressure does not justify the observed difference, 2 hrs should be more than enough to generate at least a fraction of non reaggregating monomeric aS form. The complete reversibility of the HP induced unfolding of fibrillary aS is more likely due to the use of a different starting form (strain) of aS. An issue that should be further explored also in view of its important pathophysiological implication recently reported(17).

Conclusions

Our data describe the high pressure dissociation of *wt* aS fibrils and compare it to the dissociation process triggered by proteins charge tuning. Fibrils can be disassembled at high pressure into stable random structures going through intermediate partially folded states. Interestingly, internal conversion processes among β -sheet species are observed. Conversely, fibrils subjected to alkaline environment dissociate in one step and undergo further aggregation into amorphous structures possibly generated through the interaction among carboxyl groups of acidic side chains. The two strategically designed chimeric mutants aS(1-99) and syn-syn covalent dimers behave differently at high pressure. We found that the dissociation process of syn-syn fibrils has similar characteristics to the one of *wt* aS, while β -sheet in aS(1-99) fibrils were found to be more resistant to pressure. This piece of evidence could be ascribed to a different spatial arrangement of the β -sheet elements found in the deletion mutant, an observation that may be of relevance in further analysis of the model mutants and Caspase-1 generated C-term truncated variants of aS(53) .

Authors contributions

F.P., N.P., M.O., L.B. designed research; F.P., N.P., M.O., I.T. performed research; F.S., M.B., P.M., V.M., S.L., A.P. contributed analytic tools; F.P., N.P., F.S., M.B., P.M., V.M., S.L., A.P. analysed data; F.P., N.P., L.B. wrote the manuscript.

Acknowledgement

The University of Padova for the “Prg di Ateneo” awarded to L.B., L.B. acknowledge Italian Ministry of Education, University, and Research (MIUR) - Research Projects of National Interest (PRIN) 2015 prot. 2015T778JW.

REFERENCES

1. Davidson, W.S., A Jonas, D.F. Clayton, and J.M. George. 1998. Stabilization of alpha-synuclein secondary structure upon binding to synthetic membranes. *J Biol Chem.* 273: 9443–9.
2. Weinreb, P.H., W. Zhen, A.W. Poon, K. a. Conway, and P.T. Lansbury. 1996. NACP, a protein implicated in Alzheimer's disease and learning, is natively unfolded. *Biochemistry.* 35: 13709–13715.
3. Bartels, T., J.G. Choi, and D.J. Selkoe. 2011. α -Synuclein occurs physiologically as a helically folded tetramer that resists aggregation. *Nature.* 477: 107–110.
4. Dedmon, M.M., K. Lindorff-Larsen, J. Christodoulou, M. Vendruscolo, and C.M. Dobson. 2005. Mapping long-range interactions in α -synuclein using spin-label NMR and ensemble molecular dynamics simulations. *J Am Chem Soc.* 127: 476–477.
5. Theillet, F.-X., A. Binolfi, B. Bekei, A. Martorana, H.M. Rose, M. Stuiver, S. Verzini, D. Lorenz, M. van Rossum, D. Goldfarb, and P. Selenko. 2016. Structural disorder of monomeric α -synuclein persists in mammalian cells. *Nature.* 530: 45–50.
6. Scott, D., and S. Roy. 2012. Alpha-Synuclein Inhibits Intersynaptic Vesicle Mobility and Maintains Recycling-Pool Homeostasis. *J Neurosci.* 32: 10129–10135.
7. Nemani, V.M., W. Lu, V. Berge, K. Nakamura, B. Onoa, M.K. Lee, F.A. Chaudhry, R.A. Nicoll, and R.H. Edwards. 2010. Increased Expression of alpha-Synuclein Reduces Neurotransmitter Release by Inhibiting Synaptic Vesicle Reclustering after Endocytosis. *Neuron.* 65: 66–79.
8. Burré, J., M. Sharma, T. Tsetsenis, V. Buchman, M.R. Etherton, and T.C. Südhof. 2010. Alpha-synuclein promotes SNARE-complex assembly in vivo and in vitro. *Science.* 329: 1663–1667.
9. Clayton, D.F., and J.M. George. 1999. Synucleins in synaptic plasticity and neurodegenerative disorders. *J Neurosci Res.* 58: 120–129.
10. Arima, K., K. Uéda, N. Sunohara, S. Hirai, Y. Izumiyama, H. Tono-zuka-Uehara, and M. Kawai. 1998. Immunoelectron-microscopic demonstration of NACP/ α -synuclein-epitopes on the filamentous component of Lewy bodies in Parkinson's disease and in dementia with Lewy bodies. *Brain Res.* 808: 93–100.
11. Spillantini, M.G., M.L. Schmidt, V.M. Lee, J.Q. Trojanowski, R. Jakes, and M. Goedert. 1997. Alpha-synuclein in Lewy bodies. *Nature.* 388: 839–840.
12. John Q. Trojanowski, V.M.-Y.L. 2003. Parkinson's disease and related alpha-synucleinopathies are brain amyloidoses. *Ann NY Acad Sci.* 991: 107–110.
13. Serpell, L.C., J. Berriman, R. Jakes, M. Goedert, and R. a Crowther. 2000. Fiber diffraction of synthetic alpha-synuclein filaments shows amyloid-like cross-beta conformation. *Proc Natl Acad Sci U S A.* 97: 4897–4902.
14. Tuttle, M.D., G. Comellas, A.J. Nieuwkoop, D.J. Covell, D.A. Berthold, K.D. Kloepper, J.M. Courtney, J.K. Kim, A.M. Barclay, A. Kendall, W. Wan, G. Stubbs, C.D. Schwieters, V.M.Y. Lee, J.M. George, and

- C.M. Rienstra. 2016. Solid-state NMR structure of a pathogenic fibril of full-length human α -synuclein. *Nat Struct Mol Biol.* 23: 1–9.
15. Vilar, M., H.T. Chou, T. Lührs, S.K. Maji, D. Riek-Loher, R. Verel, G. Manning, H. Stahlberg, and R. Riek. 2008. The fold of α -synuclein fibrils. *Proc Natl Acad Sci.* 105: 8637–8642.
 16. Rodriguez, J. a, M.I. Ivanova, M.R. Sawaya, D. Cascio, F.E. Reyes, D. Shi, S. Sangwan, E.L. Guenther, L.M. Johnson, M. Zhang, L. Jiang, M. a Arbing, B.L. Nannenga, J. Hattne, J. Whitelegge, A.S. Brewster, M. Messerschmidt, S. Boutet, N.K. Sauter, T. Gonen, and D.S. Eisenberg. 2015. Structure of the toxic core of α -synuclein from invisible crystals. *Nature. advance on:* 486–490.
 17. Peelaerts, W., L. Bousset, A. Moskalyuk, R. Pulizzi, M. Giugliano, R. Melki, and V. Baekelandt. 2015. Alpha-Synuclein strains cause distinct synucleinopathies after local and systemic administration. *Nature.* 522: 340–344.
 18. Plotegher, N., E. Greggio, M. Bisaglia, and L. Bubacco. 2014. Biophysical groundwork as a hinge to unravel the biology of α -synuclein aggregation and toxicity. *Q Rev Biophys.* 1: 1–48.
 19. Winner, B., R. Jappelli, S.K. Maji, P.A. Desplats, L. Boye, S. Aigner, C. Hetzer, T. Loher, M. Vilar, S. Campioni, C. Tzitzilonis, A. Soragni, S. Jessberger, H. Mira, A. Consiglio, E. Pham, E. Masliah, F.H. Gage, and R. Riek. 2011. In vivo demonstration that α -synuclein oligomers are toxic. *Proc Natl Acad Sci.* 108: 4194–4199.
 20. Osterberg, V., K. Spinelli, L. Weston, K. Luk, R. Woltjer, and V. Unni. 2015. Progressive Aggregation of Alpha-Synuclein and Selective Degeneration of Lewy Inclusion-Bearing Neurons in a Mouse Model of Parkinsonism. *Cell Rep.* 10: 1252–1260.
 21. Kim, H.-Y., M.-K. Cho, a Kumar, E. Maier, C. Siebenhaar, S. Becker, C.O. Fernandez, H. a Lashuel, R. Benz, and a Lange. 2009. Structural Properties of Pore-Forming Oligomers of alpha -Synuclein. *J- Amer Chem Soc.* 131: 17482–17489.
 22. Shammas, S.L., T.P.J. Knowles, A.J. Baldwin, C.E. MacPhee, M.E. Welland, C.M. Dobson, and G.L. Devlin. 2011. Perturbation of the stability of amyloid fibrils through alteration of electrostatic interactions. *Biophys J.* 100: 2783–2791.
 23. Cohlberg, J. a., J. Li, V.N. Uversky, and A.L. Fink. 2002. Heparin and other glycosaminoglycans stimulate the formation of amyloid fibrils from alpha-synuclein in vitro. *Biochemistry.* 41: 1502–1511.
 24. Nath, S., J. Meuvius, J. Hendrix, S. a. Carl, and Y. Engelborghs. 2010. Early aggregation steps in alpha-synuclein as measured by FCS and FRET: Evidence for a contagious conformational change. *Biophys J.* 98: 1302–1311.
 25. Kim, H.Y., M.K. Cho, D. Riedel, C.O. Fernandez, and M. Zweckstetter. 2008. Dissociation of amyloid fibrils of alpha-synuclein in supercooled water. *Angew Chemie - Int Ed.* 47: 5046–5048.
 26. Ikenoue, T., Y.H. Lee, J. Kardos, M. Saiki, H. Yagi, Y. Kawata, and Y. Goto. 2014. Cold denaturation of

- alpha-synuclein amyloid fibrils. *Angew Chemie - Int Ed.* 53: 7799–7804.
27. Foguel, D., M.C. Suarez, A.D. Ferrão-Gonzales, T.C.R. Porto, L. Palmieri, C.M. Einsiedler, L.R. Andrade, H. a Lashuel, P.T. Lansbury, J.W. Kelly, and J.L. Silva. 2003. Dissociation of amyloid fibrils of alpha-synuclein and transthyretin by pressure reveals their reversible nature and the formation of water-excluded cavities. *Proc Natl Acad Sci U S A.* 100: 9831–9836.
 28. Piccirilli, F., S. Mangialardo, P. Postorino, L. Baldassarre, S. Lupi, and A. Perucchi. 2012. Sequential dissociation of insulin amyloids probed by high pressure Fourier transform infrared spectroscopy. *Soft Matter.* : 11863–11870.
 29. Piccirilli, F., S. Mangialardo, P. Postorino, S. Lupi, and a. Perucchi. 2013. FTIR analysis of the high pressure response of native insulin assemblies. *J Mol Struct.* 1050: 159–165.
 30. De Oliveira, G.A.P., M.D.A. Marques, C. Cruzeiro-silva, Y. Cordeiro, C. Schuabb, A.H. Moraes, R. Winter, H. Oshkinat, D. Foguel, M.S. Freitas, and J.L. Silva. 2016. Structural basis for the dissociation of alpha-synuclein fibrils triggered by pressure perturbation of the hydrophobic core. *Sci Rep.* 6: 37990.
 31. Grigera, J.R., and A.N. McCarthy. 2010. The behavior of the hydrophobic effect under pressure and protein denaturation. *Biophys J.* 98: 1626–1631.
 32. Pivato, M., G. De Franceschi, L. Tosatto, E. Frare, D. Kumar, D. Aioanei, M. Brucale, I. Tessari, M. Bisaglia, B. Samori, P.P. de Laureto, and L. Bubacco. 2012. Covalent alpha-Synuclein Dimers: Chemical-Physical and Aggregation Properties. *PLoS One.* 7.
 33. Plotegher, N., D. Kumar, I. Tessari, M. Brucale, F. Munari, L. Tosatto, E. Belluzzi, E. Greggio, M. Bisaglia, S. Capaldi, D. Aioanei, S. Mammi, H.L. Monaco, B. Samo, and L. Bubacco. 2014. The chaperone-like protein 14-3-3 η interacts with human α -synuclein aggregation intermediates rerouting the amyloidogenic pathway and reducing α -synuclein cellular toxicity. *Hum Mol Genet.* : 1–38.
 34. Bortolus, M., F. Tombolato, I. Tessari, M. Bisaglia, S. Mammi, L. Bubacco, A. Ferrarini, and A.L. Maniero. 2008. Broken helix in vesicle and micelle-bound alpha-synuclein: Insights from site-directed spin labeling-EPR experiments and MD simulations. *J Am Chem Soc.* 130: 6690–6691.
 35. Piccirilli, F., G. Schirò, V. Vetri, S. Lupi, A. Perucchi, and V. Militello. 2015. Decoding vibrational states of Concanavalin A amyloid fibrils. *Biophys Chem.* 199: 17–24.
 36. Barth, A. 2000. The infrared absorption of amino acid side chains. *Prog Biophys Mol Biol.* 74: 141–173.
 37. Winter, R., M. Pühse, and J. Markgraf. 2011. High-Pressure Vibrational Spectroscopy Studies of the Folding, Misfolding and Amyloidogenesis of Proteins. In: *Protein Folding and Misfolding Shining light by Infrared Spectroscopy.* . pp. 117–146.
 38. Zurdo, J., J.I. Guijarro, and C.M. Dobson. 2001. Preparation and characterization of purified amyloid

- fibrils. *J Am Chem Soc.* 123: 8141–8142.
39. Gerwert, K., G. Souvignier, and B. Hess. 1990. Simultaneous monitoring of light-induced changes in protein side-group protonation, chromophore isomerization, and backbone motion of bacteriorhodopsin by time-resolved Fourier-transform infrared spectroscopy. *Proc Natl Acad Sci U S A.* 87: 9774–8.
 40. Barth, A. 2000 The infrared absorptions of amino acid side chains. *Progress in Biophysics and Molecular Biology* 74 :141-173
 41. Fabian, H. and Mantele, W. (2001), *Infrared Spectroscopy of Proteins*. In Chalmers, J.M. and Griffiths, P.R.; *Handbook of Vibrational Spectroscopy* (Vol. 5). New York (NY): WILEY.
 42. Carulla, N., G.L. Caddy, D.R. Hall, J. Zurdo, M. Gairí, M. Feliz, E. Giralt, C. V Robinson, and C.M. Dobson. 2005. Molecular recycling within amyloid fibrils. *Nature.* 436: 554–8.
 43. Hillson, N., J.N. Onuchic, and a E. García. 1999. Pressure-induced protein-folding/unfolding kinetics. *Proc Natl Acad Sci U S A.* 96: 14848–14853.
 44. Comellas, G., L.R. Lemkau, A.J. Nieuwkoop, K.D. Kloepper, D.T. Lador, R. Ebisu, W.S. Woods, A.S. Lipton, J.M. George, and C.M. Rienstra. 2011. Structured regions of alpha-Synuclein fibrils include the early-onset Parkinson's disease mutation sites. *J Mol Biol.* 411: 881–895.
 45. Apetri, M.M., N.C. Maiti, M.G. Zagorski, P.R. Carey, and V.E. Anderson. 2006. Secondary structure of alpha-synuclein oligomers: Characterization by Raman and atomic force microscopy. *J Mol Biol.* 355: 63–71.
 46. Ahmad, B., Y. Chen, and L.J. Lapidus. 2012. Aggregation of -synuclein is kinetically controlled by intramolecular diffusion. *Proc Natl Acad Sci.* 109: 2336–2341.
 47. Krishnan, S., E.Y. Chi, S.J. Wood, B.S. Kendrick, C. Li, W. Garzon-Rodriguez, J. Wypych, T.W. Randolph, L.O. Narhi, A.L. Biere, M. Citron, and J.F. Carpenter. 2003. Oxidative dimer formation is the critical rate-limiting step for Parkinson's disease alpha-synuclein fibrillogenesis. *Biochemistry.* 42: 829–837.
 48. Takahashi, T., H. Yamashita, T. Nakamura, Y. Nagano, and S. Nakamura. 2002. Tyrosine 125 of α -synuclein plays a critical role for dimerization following oxidative stress. *Brain Res.* 938: 73–80.
 49. Souza, M., B.I. Giasson, Q. Chen, V.M. Lee, and H. Ischiropoulos. 2000. Dityrosine Cross-linking Promotes Formation of Stable alpha-Synuclein Polymers IMPLICATION OF OXIDATIVE STRESS IN THE PATHOGENESIS OF. *J Biol Chem.* 275: 18344–18349.
 50. Murray, I.V.J., Giasson, B.I., S.M. Quinn, V. Koppaka, P.H. Axelsen, H. Ischiropoulos, J.Q. Trojanowski, and V.M.-Y. Lee. 2003. C-terminal truncation: Role of alpha-synuclein carboxy-terminus on fibril formation in vitro. *Biochemistry.* 42: 8530–8540.
 51. Qin, Z., D. Hu, S. Han, D.-P. Hong, and A.L. Fink. 2007. Role of different regions of alpha-synuclein in the assembly of fibrils. *Biochemistry.* 46: 13322–13330.
 52. Khurana, R., C. Ionescu-zanetti, M. Pope, J. Li, L. Nielson, M. Ramı, L. Regan, A.L. Fink, and S.A. Carter.

2003. A General Model for Amyloid Fibril Assembly Based on Morphological Studies Using Atomic Force Microscopy. *Biophys J.* 85: 1135–1144.

53. Bassil, F., Fernagut, P.O., Bezard E., Pruvost A., Leste-Lasserre T., Hoang Q.Q., Ringe D., Petsko G.A., Meissner W.G. 2016. Reducing C-terminal truncation mitigates synucleinopathy and neurodegeneration in a transgenic model of multiple system atrophy. *Proc Natl Acad Sci U S A.* 113(34):9593-8.

FIGURE LEGENDS

Figure 1. Time evolution of Amide I' spectra (from grey to black) upon HP (2.6 kbar) induced dissociation (panel A) and upon pH induced dissociation (panel B).

Amide I' 2D-correlation spectra of the HP (2.6 kbar) (panels C, E) and pH (pH 11) (panels D, F) dissociation kinetics of preformed fibrils of aS.

The correlation function is defined as $\Phi(k_1, k_2) + i\Psi(k_1, k_2)$. While the real part of the function, the synchronous spectrum (Φ), can give information on the reciprocal amplitude variation of signals, through the analysis of the imaginary part of the correlation function, the asynchronous spectrum (Ψ), it is possible to reconstruct the temporal order in which the variations highlighted by synchronous features occur.

During the dissociation induced by proteins charge redistribution occurring at pH 11 three main amide moieties can be detected: β -sheet building up the amyloid absorbing around 1617 cm^{-1} , random coil and turns absorbing in the region between $1660\text{--}1640\text{ cm}^{-1}$ (r) and aggregated strands (β^*), mainly found in the absorption region around 1685 cm^{-1} . The asynchronous spectrum Ψ of the process taking place at high pressure (2.6 kbar) shows the presence of several intermediate species. Two distinct random coil absorptions can be detected, around $1640\text{--}1642\text{ cm}^{-1}$ and around 1648 cm^{-1} and at least three intermolecular structures in β -sheet configuration around 1622 cm^{-1} , 1617 cm^{-1} and 1614 cm^{-1} .

Figure 2. Raman Amide I (panel A) and Amide III (panel B) spectra of native monomeric aS, of its fibrillar form and after alkaline pH-induced dissociation of fibrils. The peak at about 1603 cm^{-1} , ascribed to aromatic chains modes, can be clearly identified in the free monomer. Conversely, it is absent in the fibrillar sample and it is partially restored upon pH driven dissociation of fibrils. The dissociation of fibrils is suggested also by the observation of β -sheet associated signal in Amide III region at about 1230 cm^{-1} , which is only present in the fibrillar sample. Differences with native wt are found in the region of C_β modes, marking the reorder of side groups upon re-aggregation occurring after fibrils dissociation in alkaline environment. The dissociation of fibrillar β -sheet is confirmed by CD measurements (panel C) while TEM measurements show the amorphous nature of the aggregates formed upon pH driven dissociation of fibrils, with only residual

presence of small aS fibrils (D).

Figure 3: Normalized band of aS(1-99) (panel A) and syn-syn (panel B) fibrils at increasing values of pressure. β -sheet dissociation occurs in several high pressure steps and high β -sheet containing species are stabilized at high pressure. (C) Comparison of the pressure dependence of the I_{b^*} value, β -sheet intensity normalized to the isosbestic point drawn by Amide I' spectra, for aS(1-99) and syn-syn dimers.

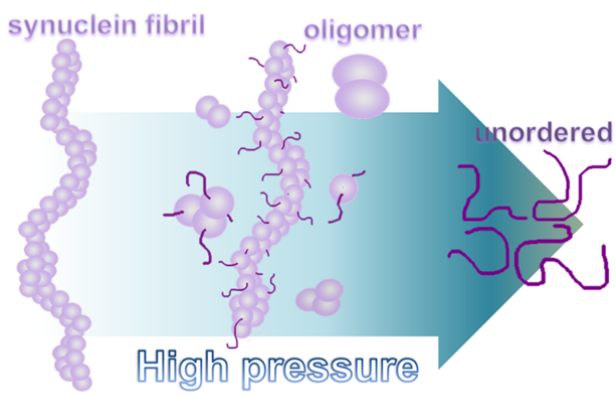
Figure 4: 2nd-derivative spectra of the Amide I' region for the two chimeric mutants measured at increasing pressure values. A fraction of β -sheet survived after pressurization of both aS(1-99) and syn-syn amyloids as revealed by the presence of 2nd-derivative minima in the region around 1620 cm^{-1} even at the highest pressure applied for both the samples. In addition aS(1-99) (full line) responds to high pressure by blue-shifting β -sheet vibrational mode at about 1622 cm^{-1} , hinting to the enhancement of the structure compactness upon compression. Conversely, syn-syn dimer (dotted line) appears rigid as no shifting modes are detected.

Table 1: Amide I' assignments for secondary structures of synuclein fibrils.

Wavenumber (cm ⁻¹)	Structure
1617	b-sheet (β_{amyloid})
1622	b-sheet ($\beta_{\text{oligomers}}$)
1640, 1645, 1648	random coil (r)
1656, 1668	turn (t) and bend (b)
1685	turn (t), lateral chains

Table 2 : Correlation analysis for HP dissociation of aS fibrils. Synchronous (Φ) and asynchronous (Ψ) correlation off-diagonal peaks signs for each frequencies couple are reported separated by commas (Φ , Ψ).

$k_2 \backslash k_1$	HP dissociation						
	1617 β_{fibril}	1622 β_{oligomer}	1640 r	1645 r	1648 r	1656 t, b	1668 t, b
1617 β_{fibril}		+, +	-, +	-, +		-, -	-, -
1622 β_{oligomer}					-, -	?	?
1640 r						+, -	
1648 r						+, -	+, -
1656 t, b							
1668 t, b							



Correlated events:

1617:1640 and 1617:1645
 β_{fibril} decreases then r increases

1617:1656 and 1617:1668
 β_{fibril} decreases then t and b increase

1617:1622
 β_{fibril} decreases then β_{oligomer} decreases

1622:1648
 β_{oligomer} decreases then r increases

1640:1656 and 1648:1656 and 1648:1668
 r increases after t and b decrease

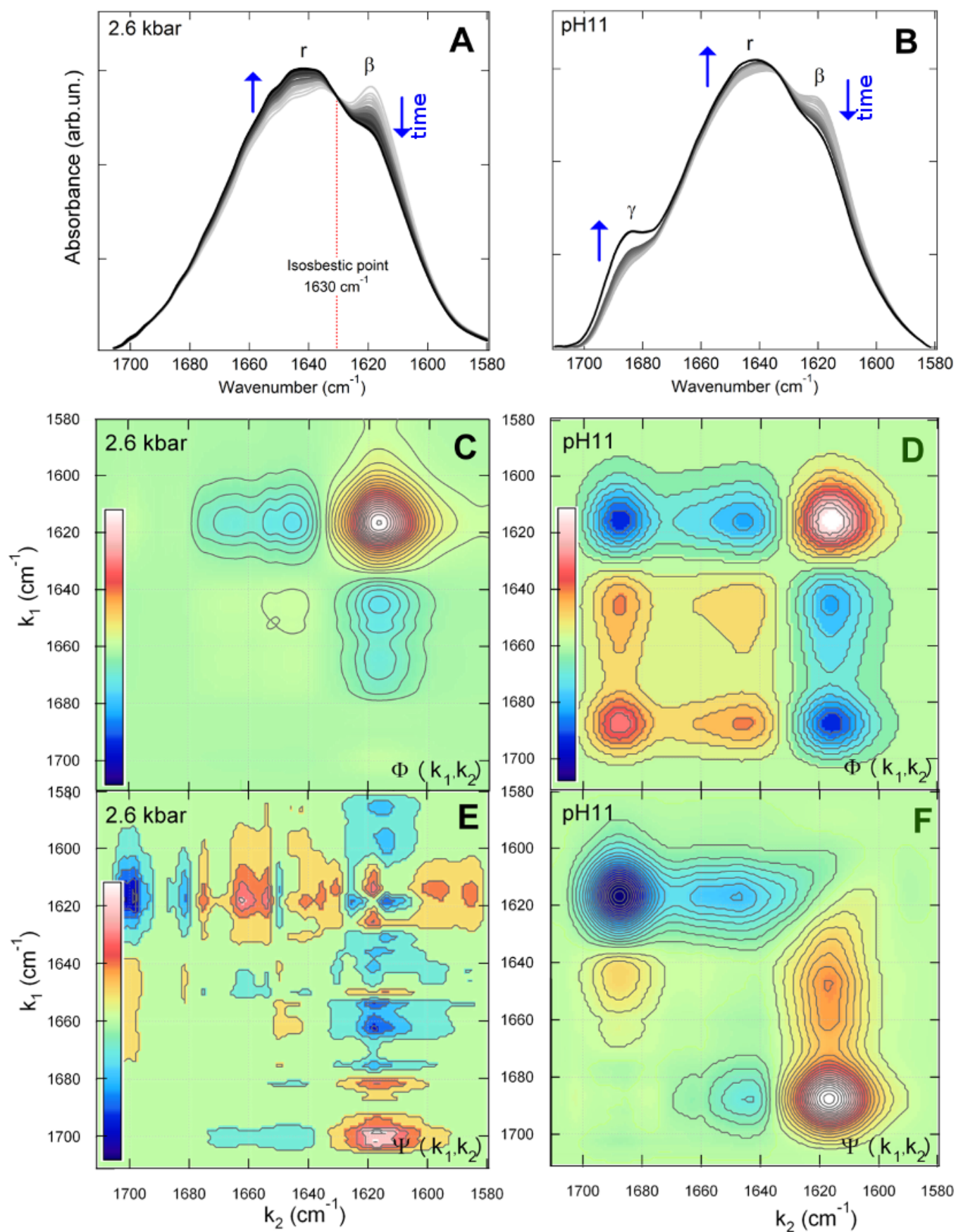


Figure 1

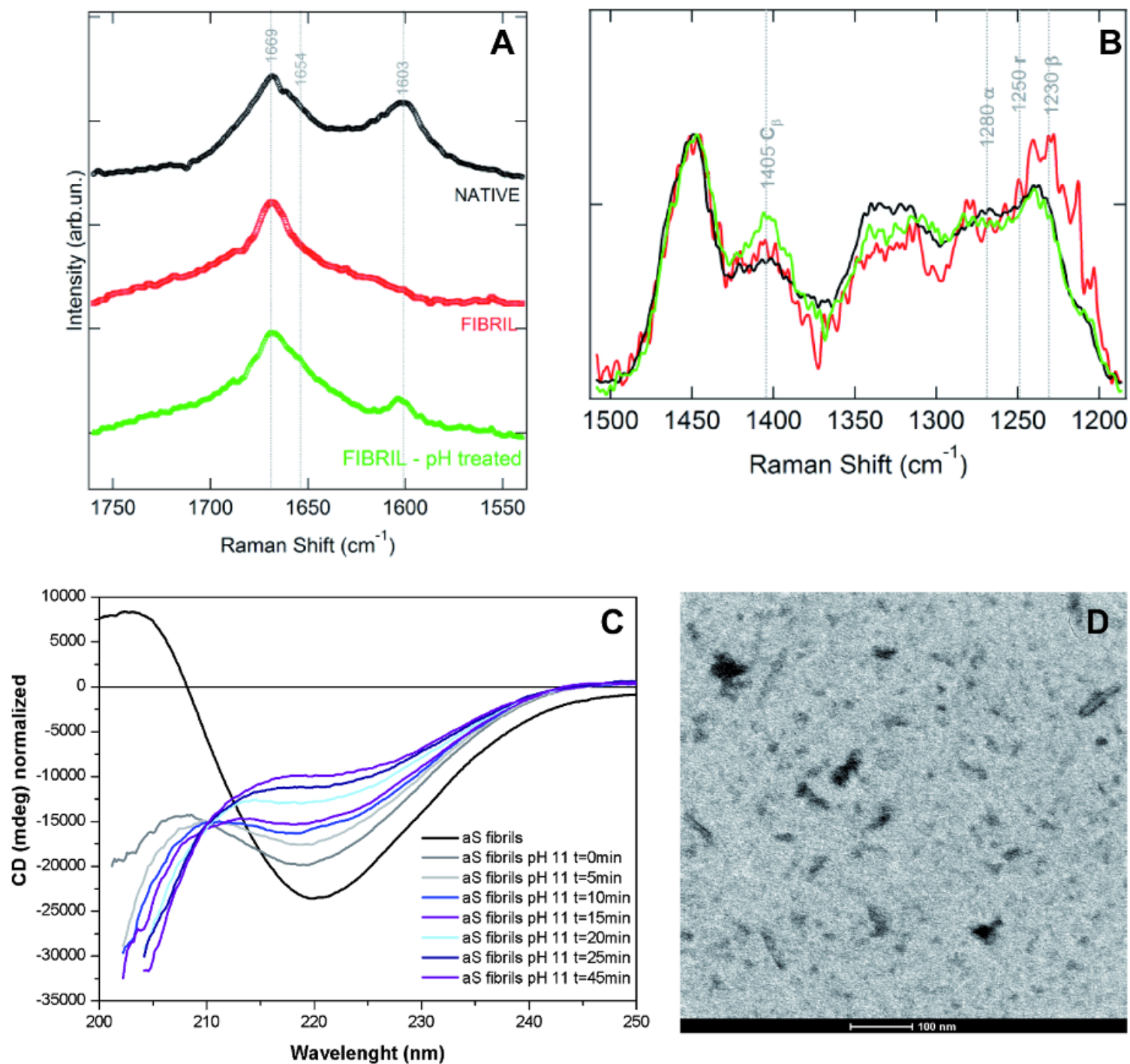


Figure 2

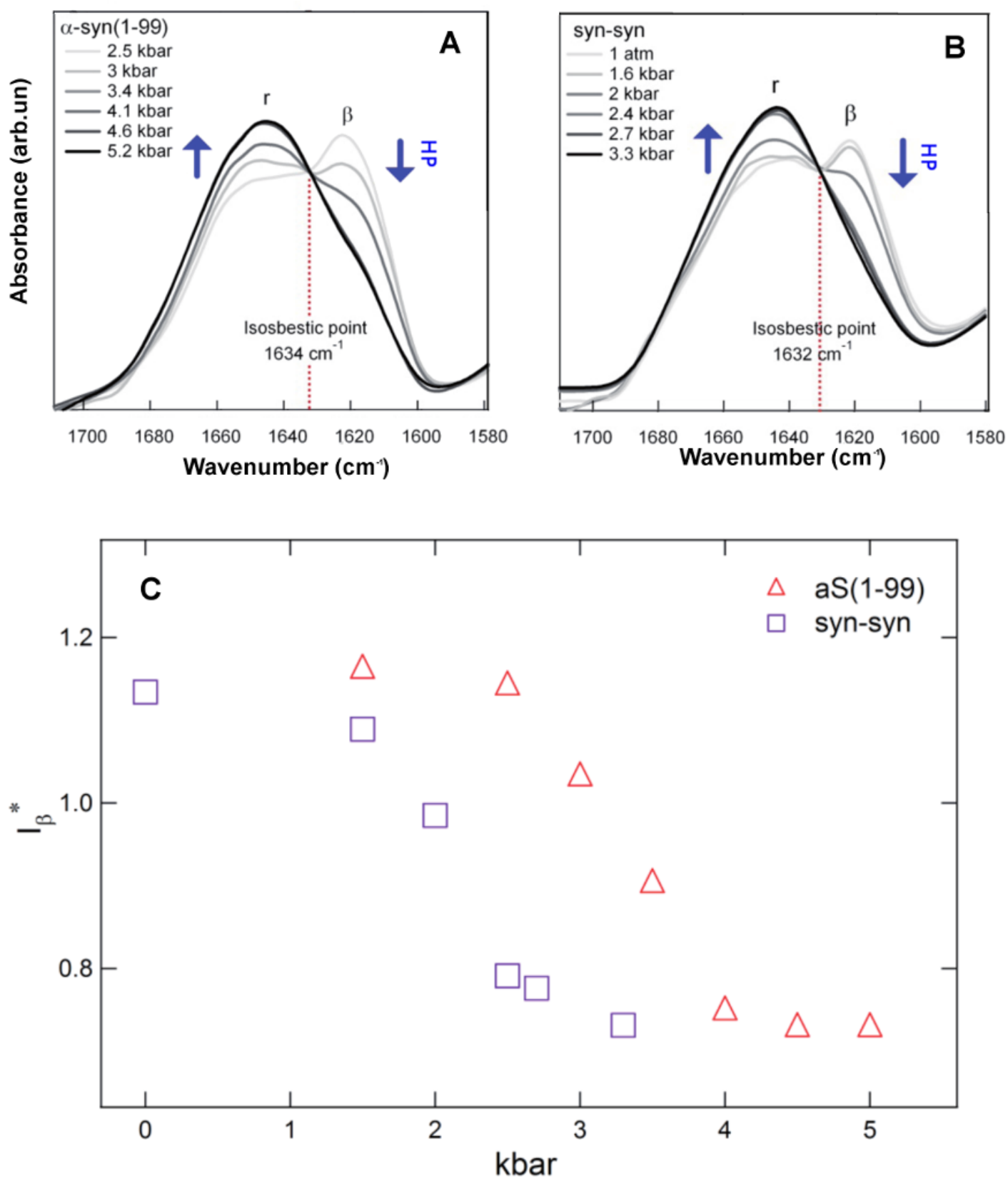


Figure 3

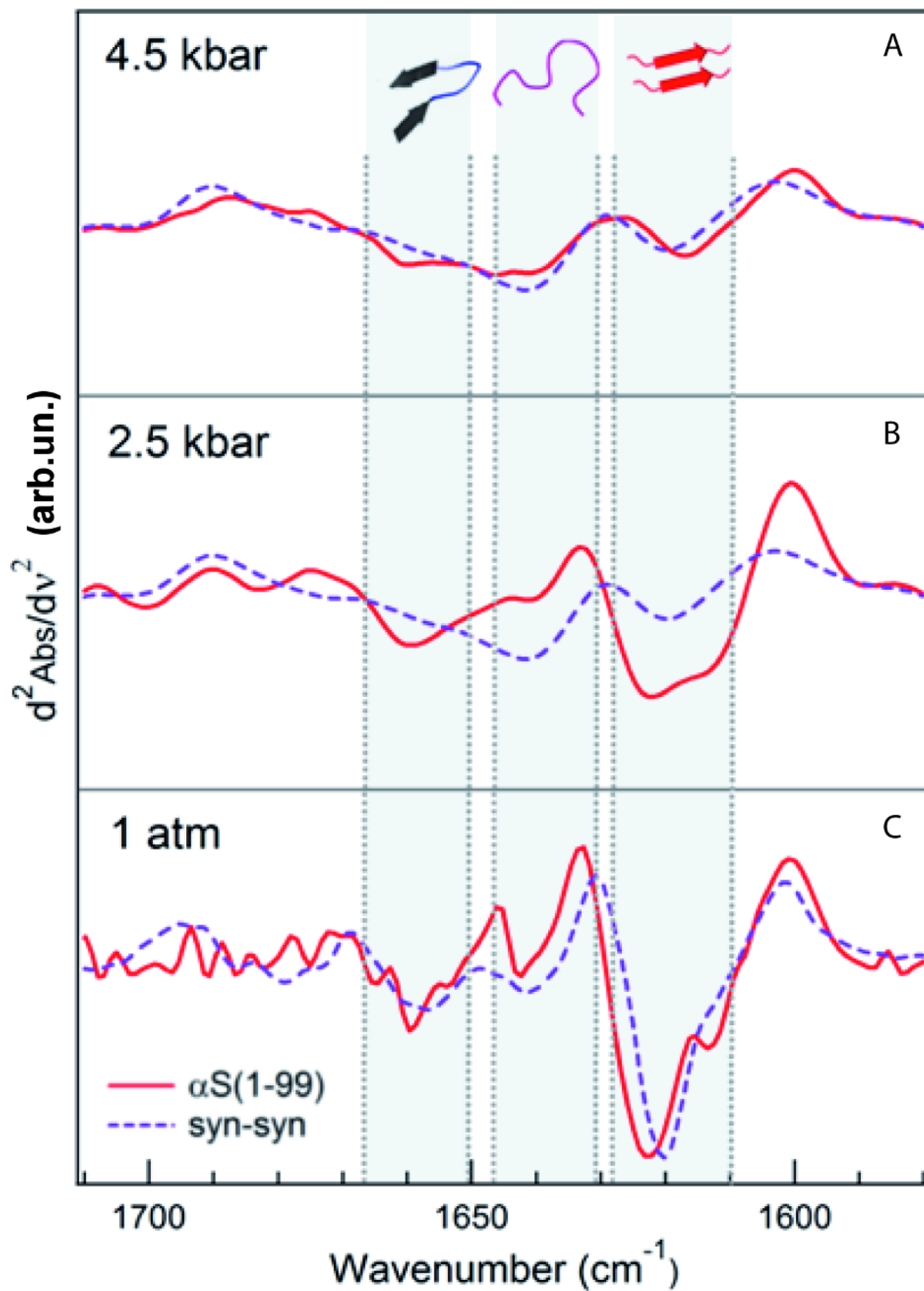


Figure 4

High Pressure driven reversible unfolding of alpha-synuclein fibrils reveals structural hierarchy in their formation

F. Piccirilli[§], N. Plategher[§], M. G. Ortore, I. Tessari, F. Spinozzi, M. Beltramini, P. Mariani, V. Militello,
S. Lupi, A. Perucchi, L. Bubacco

§ These two authors equally contributed to this work.

Supporting Information

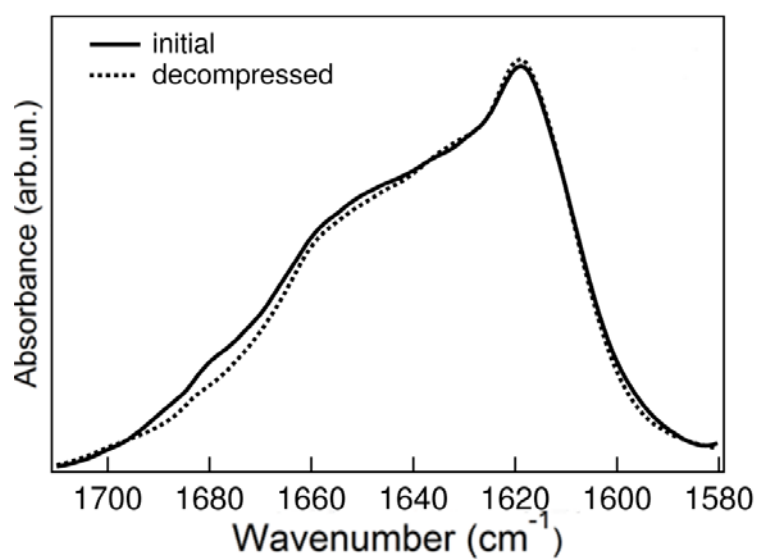


Figure S1: Amide I' band of wt aS fibrils at 1 atm measured before and after compression to 2.6 kbar. The matching of the two bands suggests the reversibility of high pressure dissociation of fibrillar β -sheet.

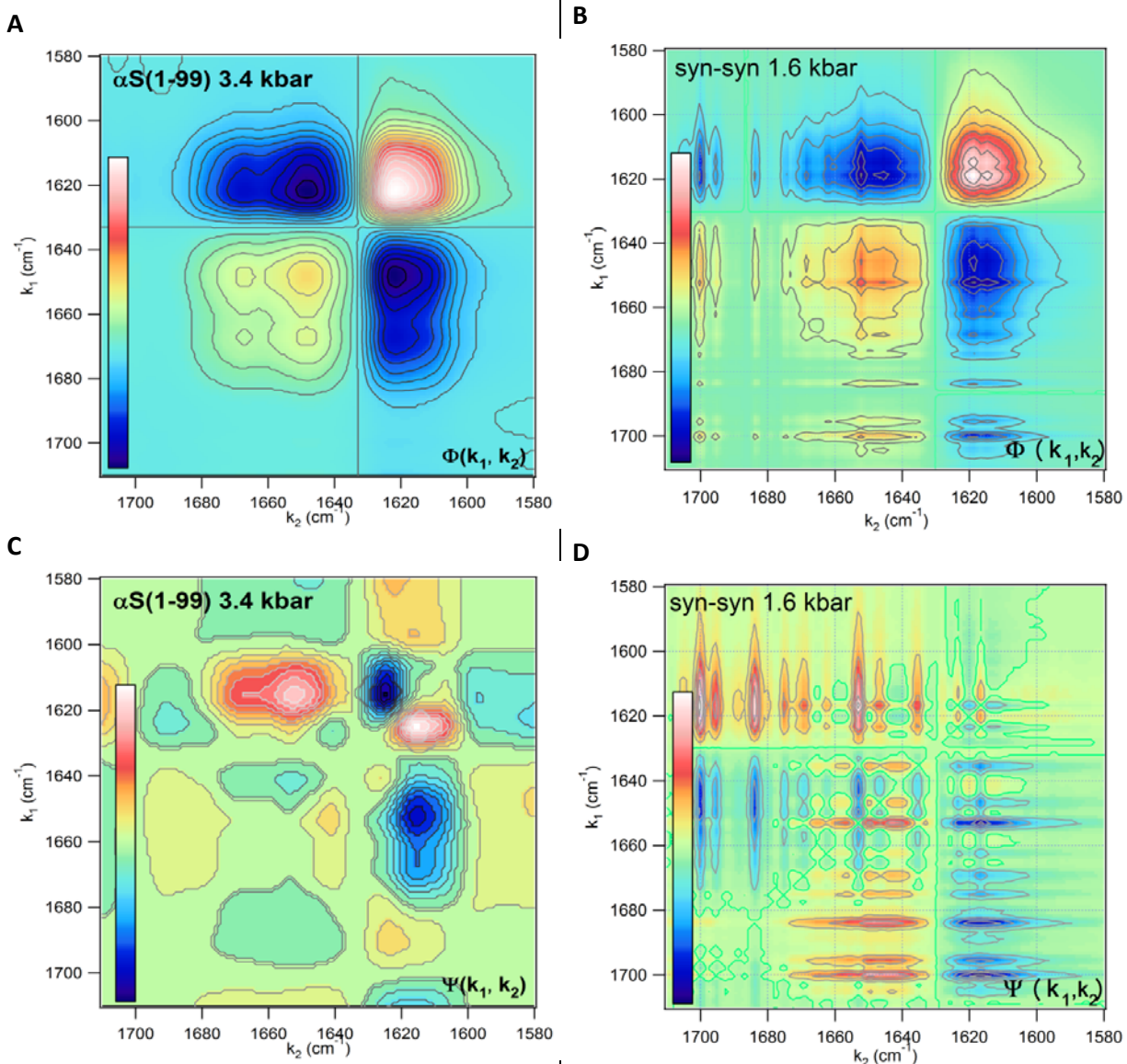


Figure S2: Synchronous and asynchronous spectra of aS(1-99) (A, C) and syn-syn (B, D) fibrils pressure driven dissociation. As it is remarked by the presence of multiple peaks in the region around 1610-1630 cm^{-1} , more than one β -sheet specie participate to the process. The presence of several intermediate intramolecular structures is also signaled by the several peaks found at higher frequencies (1640-1670 cm^{-1}) where random coils, helices, turn and loops are typically found.

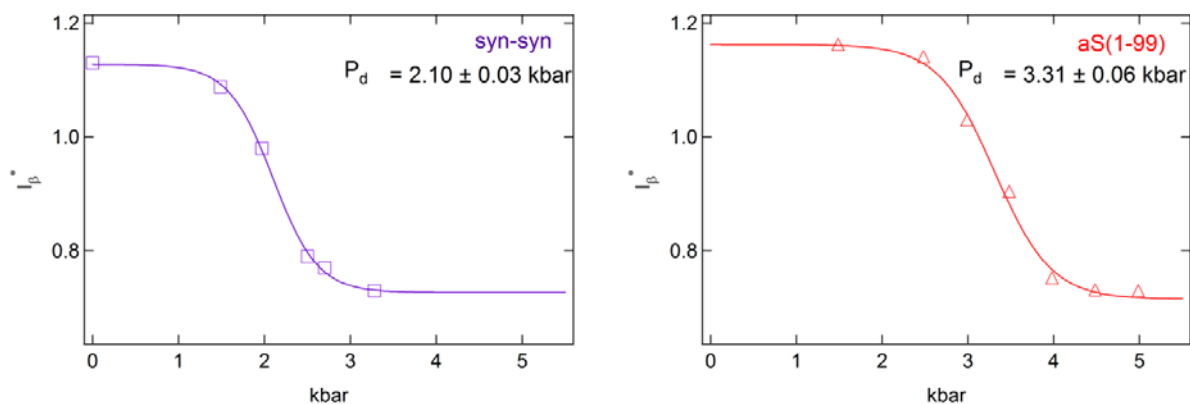


Figure S3: Experimental (markers) and fitted (lines) of I_b^* , β -sheet intensity normalized to the isosbestic point drawn by Amide I' spectra, reported in Figure 4. Data have been fitted with Sigmoid profiles following the equation: $A + B/(C + e^{(P_d-P)k})$. The fitted values of the dissociation pressure P_d are reported in the graphs.

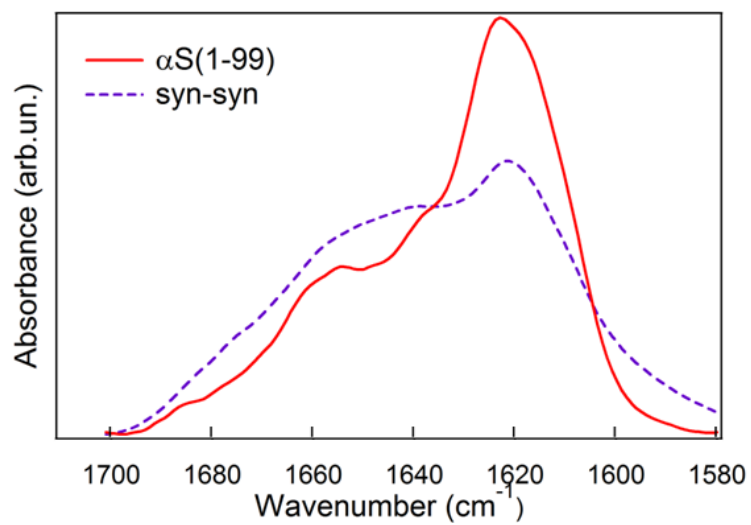


Fig. S4: Ambient pressure spectra of αS(1-99) and syn-syn fibrils in the region of Amide I' (1580-1710 cm⁻¹).

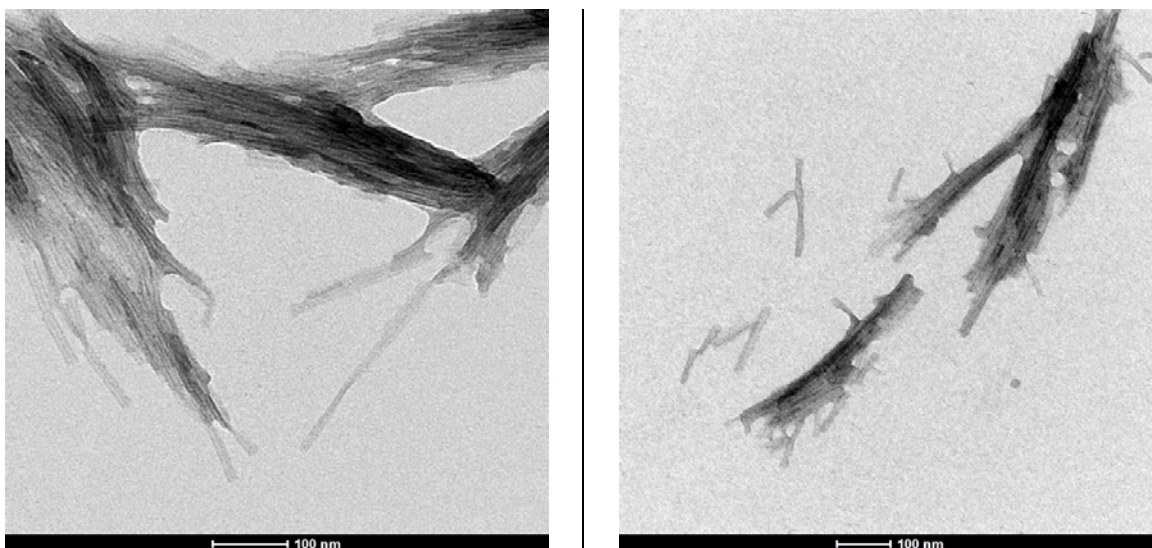


Figure S5: TEM images of aS(1-99) fibrils before (on the left) and after (on the right) a compression-decompression cycle showing a very similar morphology.